SPATIOTEMPORAL DYNAMICS IN A TWISTED, CIRCULAR WAVEGUIDE ARRAY

ROSS PARKER, YANNAN SHEN, ALEJANDRO ACEVES, AND JOHN ZWECK

Abstract. We consider the existence and spectral stability of nonlinear discrete localized solutions representing light pulses propagating in a twisted multi-core optical fiber. By considering an even number, N, of waveguides, we derive asymptotic expressions for solutions in which the bulk of the light intensity is concentrated as a soliton-like pulses confined to a single waveguide. The leading order terms obtained are in very good agreement with results of numerical computations. Furthermore, as in the model without temporal dispersion, when the twist parameter, ϕ, is given by $\phi = \pi/N$, these standing waves exhibit optical suppression, in which a single waveguide remains unexcited, to leading order. Spectral computations and numerical evolution experiments suggest that these standing wave solutions are stable for values of the coupling parameter less than a critical value, at which point a spectral instability results from the collision of an internal eigenvalue with the eigenvalues at the origin. This critical value has a maximum when $\phi = \pi/N$.

Keywords: nonlinear optics, topological photonics, nonlinear Schrödinger equation, twisted multi-core fibers, spatiotemporal localization

1. Introduction

Multi-core optical fibers, which are optical waveguides that contain multiple fiber cores within a single cladding, have important applications in diverse fields. In the linear regime, current research targets the possibility of achieving spatial division multiplexing (SDM) at telecommunication wavelengths with the goal of increasing information capacity [4]. At high intensities, in the nonlinear regime, current research includes generating high power coherent pulses by combining light propagating in each core [1]. As it relates to basic research, this optics platform presents an opportunity to theoretically [2] and experimentally [14] explore localized spatiotemporal dynamics (discrete light bullets) in nonlinear discrete systems, localized soliton-like solutions, and other structures such as discrete optical vortices [25]. While most research has been on uniform, equally spaced waveguide arrays, recent technological advances which allow for more general configurations have opened new research directions in what is called topological photonics [16]. This is the case, for example, when a twist is imposed on a circular multi-core fiber, which in particular allows for fine control of diffraction and light transfer in a similar manner to axis bending in linear waveguide arrays [10]. In the linear regime, twisted multi-core fibers have applications in distributive sensing, in which position, temperature, strain, and acoustic signals can be detected along the entire length of the fiber [27, 28]. Of particular note is shape sensing, in which the shape of the optical fiber can be reconstructed using measurements of light transmission and scattering through the fiber.

The coupled mode equations that model optical transmission in twisted, circular, multi-core fibers were derived in [12, 11, 7]. In non-dimensionalized form (and in the setting of no optical gain or loss) these equations are given by

$$i\partial_z c_n + k\left(e^{i\phi}c_{n-1} + e^{-i\phi}c_{n+1}\right) + |c_n|^2 c_n = 0, \tag{1}$$

for $n = 1, \dots, N$, where N is the number of fibers in the ring, and the indices n are taken mod N due to the circular geometry (see Figure 1). The complex amplitudes, $c_n(z)$, represent the localized field amplitude in each waveguide, the independent variable, z, is along the axis of propagation, and k is the non-dimensional strength of the nearest-neighbor coupling of the waveguides in the

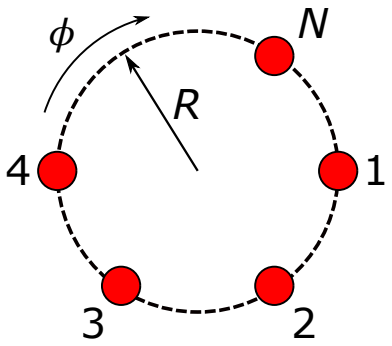

FIGURE 1. Twisted, circular, multi-core fiber consisting of N waveguides.

ring. The entire fiber structure is twisted along the propagation axis with a spatial period, Λ, and the twist parameter, $\phi = 4\pi^2\epsilon n_s R^2/N\lambda$, is the Peierls phase introduced by the twist [12, 21], where $\epsilon = 2\pi/\Lambda$ is the frequency of the twist, n_s the refractive index of the substrate, R is the radius of the circular ring, and λ is the wavelength of the propagating field [5, 20]. We note that this model only considers standing wave modes in each waveguide. When the twist parameter $\phi = 0$, the model reduces to the discrete nonlinear Schrödinger (DNLS) equation [9] on a finite, periodic lattice.

Rather than focusing on applications, the results in this paper are aimed at advancing understanding of the role that topological properties have on the dynamics of spatiotemporal localized modes. Indeed, the fiber twist permits the establishment of a topological state in the fiber, in which the intensity in one (or more) of the cores is completely suppressed. Specifically, an asymptotic analysis of the optical intensity in a six-core twisted optical fiber [5] showed that if the bulk of the optical intensity is confined to a single fiber in the ring, then the intensity in the opposite fiber in the ring is suppressed, to leading order, when $\phi = \pi/6$. This phenomenon can be interpreted as an optical analogue of Aharonov-Bohm (AB) suppression of tunneling in [15, 20, 19], in which the fiber twist plays the role of the magnetic flux in the quantum mechanical system [13]. This suppression effect was established analytically for a four-core optical fiber when $\phi = \pi/4$ in [19]. In [17] we extended this analysis to standing wave solutions of the form $c_n = a_n e^{i(\omega z+\theta_n)}$ which are constant in amplitude and oscillatory in z. We showed that when the number of fibers N is even, standing wave solutions exist in which the bulk of the intensity is contained in a single fiber core, and the intensity in the opposite core in the ring is completely suppressed for all z when $\phi = \pi/N$. Using numerical computations of spectra and evolution experiments, we showed that these standing wave solutions are stable, and we also extended these results to the case that N is odd.

In this paper, we extend these results to the pulsed regime. To do so, we incorporate a second-order temporal dispersion term, as is found in the nonlinear Schrödinger (NLS) equation, namely,

$$i\partial_z c_n + \partial_t^2 c_n + k\left(e^{i\phi}c_{n-1} + e^{-i\phi}c_{n+1}\right) + |c_n|^2 c_n = 0 \qquad n = 1, \dots, N, \tag{2}$$

where the complex amplitudes, c_n, are now functions of both z and t. Using asymptotic analysis, we derive leading order expressions for solutions in which the bulk of the intensity is contained in a single core. Since these results derive from asymptotic series expansions in the coupling parameter, k, we consider only the case of weak coupling, i.e. $k < 1$. We demonstrate that optical suppression also occurs in this model when the number of cores, N, is even, and phase parameter, ϕ, is given by $\phi = \pi/N$. Asymptotic methods have an extensive history as a tool for the analysis of lattice dynamical systems. In a set of pioneering works on the stability of discrete solitons [23] and discrete vortices [22] in DNLS, the first and second order terms in an asymptotic expansion of the excited sites in the lattice were used to obtain approximations for the eigenvalues of the linearized stability problem (see, for example, [23, Section 4]). While our work builds upon this general method, i.e.

we substitute an asymptotic series in the coupling parameter k into the lattice system, and then solve the resulting equations at each order of k, there are several key differences. First, the complex amplitudes c_n in (2) are functions of t (as well as z), thus equation (5) is a set of coupled ordinary differential equations rather than a set of coupled algebraic equations. We are able to simplify these equations using symmetries in the problem, which are a consequence of the circular geometry. In addition, we use this method to compute the first nonzero term in the asymptotic expansion at every site in the finite lattice, which allows us to obtain a leading order expression for the entire solution in the case where the bulk of the optical intensity is localized to a single site. In particular, since the opposite site in the ring will have the least optical intensity, we can use the asymptotic expansion for this opposite site to demonstrate optical suppression when $\phi = \pi/N$.

The paper is organized as follows. In section 2, we continue our discussion of the mathematical model (2) we are studying, and derive equations for pulsed solutions. In section 3, we compute the leading order terms in asymptotic expansions of pulsed solutions where the bulk of the intensity is contained in a single waveguide. Details of the computations are deferred to appendix B. In section 4, we present numerical results which validate our asymptotic solutions. In section 5, we investigate the stability of these pulsed solutions, using both spectral computations and evolution simulations, and we end with a brief concluding section which highlights directions for future research.

2. Mathematical model

We first recast the model (2) in vector form. Setting $c = (c_1, \dots, c_n)^T$, we can write (2) as

$$i\partial_z c + \partial_t^2 c + kA(\phi)c + \operatorname{diag}\left(|c_n|^2\right) c = 0, \tag{3}$$

where $\operatorname{diag}\left(|c_n|^2\right)$ is the diagonal matrix with diagonal entries $\{|c_1|^2, \dots, |c_N|^2\}$, and $A(\phi)$ is the tri-diagonal, banded matrix

$$A(\phi) = \begin{pmatrix} 0 & e^{-i\phi} & & \dots & e^{i\phi} \\ e^{i\phi} & 0 & e^{-i\phi} & & \\ & \ddots & \ddots & \ddots & \\ & & e^{i\phi} & 0 & e^{-i\phi} \\ e^{-i\phi} & \dots & & e^{i\phi} & 0 \end{pmatrix}. \tag{4}$$

We are interested in finding localized, pulse-like solutions of the form, $c_n(z,t) = C_n(t)e^{i\omega z}$, which are oscillatory in z with wavenumber ω, and have complex amplitude, $C_n(t)$. Substituting this ansatz into (2), the amplitudes $C_n = C_n(t)$ satisfy the system of N coupled ordinary differential equations

$$\partial_t^2 C_n + k\left(e^{i\phi}C_{n-1} + e^{-i\phi}C_{n+1}\right) + |C_n|^2 C_n - \omega C_n = 0, \tag{5}$$

where the subscripts n are taken mod N. Letting $C = (C_1, \dots, C_n)^T$, we can write this in matrix form as

$$\partial_t^2 C + kA(\phi)C + \operatorname{diag}\left(|C_n|^2\right) C - \omega C = 0. \tag{6}$$

When the coupling parameter is $k = 0$, which is known as the anti-continuum (AC) limit [3, 9], equation (6) reduces to N independent copies of the stationary NLS equation, so that the stationary solution at each site is either 0 or the NLS soliton

$$\psi(t) = \sqrt{2\omega}\operatorname{sech}(\sqrt{\omega}t). \tag{7}$$

Due to the gauge symmetry of NLS, we can multiply (7) by $e^{i\theta}$ for any θ.

To properly address the role of the twist, we incorporate a possible nontrivial time dependence to the phase of the field C_n as

$$C_n(t) = a_n(t)e^{i\theta_n(t)}, \tag{8}$$

where we have separated each complex field $C_n(t)$ into its real amplitude, $a_n(t)$, and phase, $\theta_n(t)$. Substituting (8) into (5), we obtain the equation

$$\begin{aligned} &e^{i\theta_n}\left[(\ddot{a}_n - a_n(\dot{\theta}_n)^2) + i(a_n\ddot{\theta}_n + 2\dot{a}_n\dot{\theta}_n)\right] \\ &\quad + k\left(e^{i\phi}a_{n-1}e^{i\theta_{n-1}} + e^{-i\phi}a_{n+1}e^{i\theta_{n+1}}\right) + |a_n|^2 a_n e^{i\theta_n} - \omega a_n e^{i\theta_n} = 0, \end{aligned}$$

where we have suppressed the dependence on t. Dividing by $e^{i\theta_n}$, we obtain

$$\begin{aligned} &(\ddot{a}_n - a_n(\dot{\theta}_n)^2) + i(a_n\ddot{\theta}_n + 2\dot{a}_n\dot{\theta}_n) \\ &\quad + k\left(a_{n-1}e^{-i[(\theta_n-\theta_{n-1})-\phi]} + a_{n+1}e^{i[(\theta_{n+1}-\theta_n)-\phi]}\right) + a_n^3 - \omega a_n = 0, \end{aligned} \tag{9}$$

which we can split up into real and imaginary parts to obtain the system of $2N$ coupled, real-valued ordinary differential equations

$$\ddot{a}_n - a_n(\dot{\theta}_n)^2 + k\left(a_{n-1}\cos[(\theta_n - \theta_{n-1}) - \phi] + a_{n+1}\cos[(\theta_{n+1} - \theta_n) - \phi]\right) + a_n^3 - \omega a_n = 0 \tag{10}$$

$$a_n\ddot{\theta}_n + 2\dot{a}_n\dot{\theta}_n + k\left(-a_{n-1}\sin[(\theta_n - \theta_{n-1}) - \phi] + a_{n+1}\sin[(\theta_{n+1} - \theta_n) - \phi]\right) = 0. \tag{11}$$

3. Asymptotic analysis

We use an asymptotic approach to find highly localized solutions. To do so, we assume that the bulk of the energy is concentrated in a single pulse propagating in one core, which we will call the primary node and label $n = 0$. Furthermore, we only consider the case where the number of waveguides, N, is even. We call the waveguide directly opposite the primary core the opposite core, which we label $n = N/2$. The remaining nodes in the ring are labeled $\pm n$, for $n = 1, \ldots, N/2 - 1$, where we count clockwise around the ring for positive n and counterclockwise for negative n. See Figure 2 for the labeling scheme for $N = 6$. Numerical parameter continuation experiments suggest that for N even, there exist solutions with the following symmetries (see Figure 2 for an illustration when $N = 6$):

$$\begin{aligned} a_{-n}(t) &= a_n(t) && n = 1, \ldots, N/2 \\ \theta_{-n}(t) &= -\theta_n(t) && n = 1, \ldots, N/2 \\ \theta_0(t) &= 0 \\ \theta_{N/2}(t) &= 0. \end{aligned} \tag{12}$$

We verify in appendix A that these symmetry conditions are consistent with (9), and we will look for a solution with these specific symmetries.

To find a leading order approximation for a solution to (9), we assume that the amplitudes $a_n(t)$ and phases $\theta_n(t)$ have power series expansions in the coupling parameter k, where we take $0 \leq k < 1$. Furthermore, we assume that these terms have the following orders of magnitude in k, which are suggested by numerical parameter continuation experiments:

$$\begin{aligned} a_0(t) &= \psi(t) + \mathcal{O}(k) \\ a_n(t) &= \mathcal{O}(k^n) && n = 1, \ldots, N/2 \\ \theta_n(t) &= n\phi + \mathcal{O}\left(k^{N-2n}\right) && n = 1, \ldots, N/2 - 1. \end{aligned} \tag{13}$$

Since we wish node 0 to contain the bulk of the intensity, the leading order term for $a_0(t)$ is the NLS soliton $\psi(t)$, and the rest of the terms are of order k or higher. The form of equation (9) suggests that $a_n = \mathcal{O}(ka_{n-1})$, from which we obtain the ansatz for a_n in (13). It follows from the ansatz for θ_n that, for $n = 1, \ldots, N/2 - 1$, we have $\theta_n - \theta_{n-1} - \phi = \mathcal{O}\left(k^{N-2n}\right)$. This implies that, to leading order, the cosine terms in (10) and the sine terms in (11) are 1 and 0, respectively.

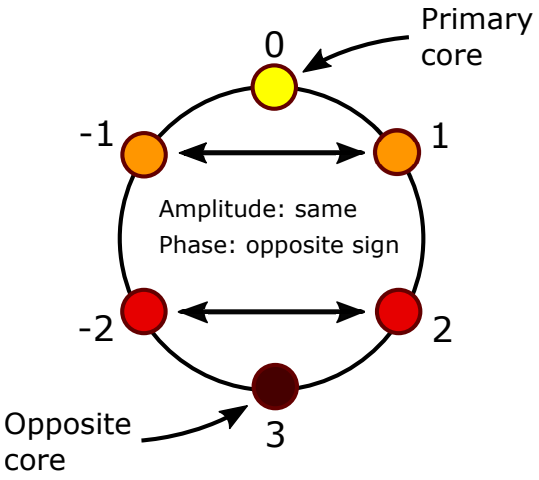

FIGURE 2. Symmetry relations and site labeling in a twisted, circular, multi-core fiber consisting of 6 waveguides.

3.1. **Asymptotic formulae.** Following the procedure detailed in appendix B, we obtain a solution to (9) of the form

$$\begin{aligned} a_0 &= \psi + k^2\widetilde{a}_0 + \mathcal{O}(k^3) \\ a_n &= k^n\widetilde{a}_n + \mathcal{O}(k^{n+2}) \qquad\qquad n = 1,\dots,N/2 \\ \theta_n &= n\phi + k^{N-2n}\widetilde{\theta}_n + \mathcal{O}(k^{N-2n+1}) \quad n = 1,\dots,N/2-1, \end{aligned} \tag{14}$$

where $\widetilde{a}_n$ is defined recursively as

$$\begin{aligned} \widetilde{a}_1 &= (\omega - \partial_t^2)^{-1}\psi \\ \widetilde{a}_n &= (\omega - \partial_t^2)^{-1}\widetilde{a}_{n-1} \qquad\qquad n = 2,\dots,N/2-1 \\ \widetilde{a}_{N/2} &= 2\cos(N\phi/2)(\omega - \partial_t^2)^{-1}\widetilde{a}_{N/2-1}. \end{aligned} \tag{15}$$

The remaining term, $\widetilde{a}_0$, from node 0 can be found by solving the equation

$$\left(\partial_t^2 - \omega + 3\psi^2\right)\widetilde{a}_0 = -2\widetilde{a}_1 = -2(\omega - \partial_t^2)^{-1}\psi, \tag{16}$$

with the condition that $\widetilde{a}_0 \perp \dot{\psi}$ in $L^2(\mathbb{R})$. We observe that each function $\widetilde{a}_n$ is defined in terms of $\widetilde{a}_{n-1}$, i.e. the amplitude of each waveguide is defined in terms of the waveguide which is one closer to the primary core. The invertibility of the linear operator $(\omega - \partial_t^2)$ is discussed in appendix B. Collapsing these recursion relations, we can write (15) in terms of the NLS soliton ψ as

$$\begin{aligned} \widetilde{a}_n &= (\omega - \partial_t^2)^{-n}\psi \qquad\qquad n = 1,\dots,N/2-1 \\ \widetilde{a}_{N/2} &= 2\cos(N\phi/2)(\omega - \partial_t^2)^{-N/2}\psi. \end{aligned} \tag{17}$$

Note that $\widetilde{a}_n$ does not depend on ϕ, except when $n = N/2$.

For the phases, we obtain the following recursive formulas for the products $\widetilde{a}_n\widetilde{\theta}$:

$$\begin{aligned} \widetilde{a}_{N/2-1}\widetilde{\theta}_{N/2-1} &= -\sin(N\phi/2)(\omega - \partial_t^2)^{-1}\widetilde{a}_{N/2} \\ \widetilde{a}_n\widetilde{\theta}_n &= (\omega - \partial_t^2)^{-1}\left(\widetilde{a}_{n+1}\widetilde{\theta}_{n+1}\right) \qquad n = 1,\dots,N/2-2, \end{aligned} \tag{18}$$

where each product $\widetilde{a}_n\widetilde{\theta}_n$ is defined in terms of the product $\widetilde{a}_{n+1}\widetilde{\theta}_{n+1}$, i.e. the phase of each waveguide is defined in terms of the waveguide which is one further from the primary core. Note

that these involve the terms $\widetilde{a}_n$, which were computed above. For $n = 1, \ldots, N/2-2$, we can again collapse these recurrence relations and write the expression for $\widetilde{a}_n\widetilde{\theta}_n$ in terms of $\widetilde{a}_{N/2-1}\widetilde{\theta}_{N/2-1}$ as

$$\widetilde{a}_n\widetilde{\theta}_n = (\omega - \partial_t^2)^{-(N/2-n-1)}\left(\widetilde{a}_{N/2-1}\widetilde{\theta}_{N/2-1}\right) \qquad n = 1, \ldots, N/2-2.$$

Substituting (17) for $\widetilde{a}_n$ and simplifying, we can again write everything in terms of ψ to obtain

$$\widetilde{a}_n\widetilde{\theta}_n = -\sin(N\phi)(\omega - \partial_t^2)^{-(N-n)}\psi \quad n = 1, \ldots, N/2-1. \tag{19}$$

3.2. **Optical suppression.** The results of the previous section hold for all cores in the fiber. We now present more refined results for the opposite core. When $\phi = \pi/N$, it follows from (17) that $\widetilde{a}_{N/2}(t) = 0$ for all t. Thus, as in the case without temporal dispersion, the intensity at the opposite core $n = N/2$ in the ring is suppressed at this value of the twist parameter ϕ. It is important to note, however, that this choice of ϕ only zeros out the leading order term in the asymptotic expansion (14) for $a_{N/2}$, i.e. the term of $\mathcal{O}(k^{N/2})$, which leaves us with $a_{N/2} = \mathcal{O}(k^{N/2+2})$. By examining higher order terms (see appendix B.4), we can obtain the stronger result that all terms in the asymptotic expansion are zero up to $\mathcal{O}(k^{N/2+3})$, leaving us with $a_{N/2} = \mathcal{O}(k^{N/2+4})$. The intensity at the opposite core may not be completely suppressed due to the presence of these higher order terms in the asymptotic expansion for $a_{N/2}$ that are much more difficult to compute. Similarly, it follows from (19) that $\widetilde{a}_n\widetilde{\theta}_n = 0$ for all n when $\phi = \pi/N$, which zeros out the leading order term in the expansions for θ_n for all n. These findings are confirmed numerically in the next section. We will see that numerical evidence in fact supports complete suppression of the opposite core when $\phi = \pi/N$.

4. Numerical results

For all simulations, unless otherwise indicated, we will take $N = 6$ fibers and $\omega = 1$. The choice of $N = 6$ fibers is for efficiency of computation, and to parallel what was done in [5, 17]. Results for larger N will be shown to illustrate the suppression effect in the opposite core when the twist parameter ϕ is π/N (Figure 6c). First, we construct pulse solutions to (5) by using parameter continuation from the anti-continuum (AC) limit ($k = 0$). To do this, we take $C_n = u_n + iv_n$ in (5), and separate real and imaginary parts to obtain

$$\begin{aligned}
&\partial_t^2 u_n + k\left((u_{n-1} + u_{n+1})\cos\phi - (v_{n-1} - v_{n+1})\sin\phi\right) + (u_n^2 + v_n^2)u_n - \omega u_n = 0,\\
&\partial_t^2 v_n + k\left((v_{n-1} + v_{n+1})\cos\phi + (u_{n-1} - u_{n+1})\sin\phi\right) + (u_n^2 + v_n^2)v_n - \omega v_n = 0.
\end{aligned} \tag{20}$$

Letting $u = (u_1, \ldots, u_N)^T$ and $v = (v_1, \ldots, v_N)^T$, we can write (20) in matrix form as

$$\begin{aligned}
&\partial_t^2 u + k(A_c(\phi)u - A_s(\phi)v) + \operatorname{diag}\left(u_n^2 + v_n^2\right)u - \omega u = 0,\\
&\partial_t^2 v + k(A_c(\phi)v + A_s(\phi)u) + \operatorname{diag}\left(u_n^2 + v_n^2\right)v - \omega v = 0,
\end{aligned} \tag{21}$$

where

$$A_c(\phi) = \operatorname{Re} A(\phi) = \begin{pmatrix} 0 & \cos\phi & & \dots & \cos\phi \\ \cos\phi & 0 & \cos\phi & & \\ & \ddots & \ddots & \ddots & \\ & & \cos\phi & 0 & \cos\phi \\ \cos\phi & \dots & & \cos\phi & 0 \end{pmatrix} \tag{22}$$

$$A_s(\phi) = \operatorname{Im} A(\phi) = \begin{pmatrix} 0 & -\sin\phi & & \dots & \sin\phi \\ \sin\phi & 0 & -\sin\phi & & \\ & \ddots & \ddots & \ddots & \\ & & \sin\phi & 0 & -\sin\phi \\ -\sin\phi & \dots & & \sin\phi & 0 \end{pmatrix}. \tag{23}$$

To start the continuation, we take $u_0(t) = \psi(t)$, $u_n(t) = 0$ for $n \neq 0$, and $v_n(t) = 0$ for all n, i.e. we start with a real NLS soliton in node 0, and the zero solution everywhere else. Spatial discretization is done using a Fourier spectral discretization with periodic boundary conditions on the interval $[-T, T]$, where T is chosen sufficiently large so that the tails of the localized solutions have sufficient room to decay. Unless otherwise indicated, we will take $T = 20$, and use 256 Fourier nodes per fiber core. Results of the parameter continuation for $\phi = 0.25$ are shown in Figure 3. As k increases, the intensity spreads from the primary core at $n = 0$ to the other cores in the ring (label 2 in Figure 3). A turning point is reached at a critical value k^* (approximately 0.455 in Figure 3; see Figure 4a for other values of ϕ), at which point k has reached a maximum, and all cores have equal amplitudes (label 3 in Figure 3). The parameter continuation then reverses direction. Solutions for decreasing k are the same as those for increasing k, except that the primary core is now located at $n = N/2$ (compare labels 2 and 4 in Figure 3; the amplitudes are identical but are located at different sites in the ring). This critical value k^* depends on both ϕ and ω. Numerical continuation experiments suggest that, for fixed ω, the maximum value of k^* occurs when $\phi = \pi/N$ (see Figure 4b for results for $N = 6$). Numerical continuation experiments also suggest that, for fixed ϕ, k^* is proportional to ω (Figure 4c). Parameter continuation results for larger N (up to $N = 24$) are similar; however, since the discretization requires NM points, where M is the number of Fourier nodes per waveguide, this is computationally infeasible for very large N.

Now that we have constructed solutions of (5), we show that we can attain suppression of the opposite core when $\phi = \pi/N$. In Figure 5, we show the amplitudes, a_n, and phases, θ_n, for $N = 6$ cores and $k = 0.25$, for $\phi = 0.25$ (top row) and $\phi = \pi/6$ (bottom row). As predicted, when $\phi = \pi/6$, there is significant suppression of the amplitude at the opposite core (compare Figure 5b and Figure 5e). In addition, we see that the angle deviation $\theta_n - n\phi$ is also significantly suppressed when $\phi = \pi/N$ (compare Figure 5c and Figure 5f). Although we only showed that the lowest order terms in the asymptotic expansion (14) are suppressed when $\phi = \pi/N$, numerical evidence suggests that, as in the model without temporal dispersion [17], this suppression is complete, i.e. the amplitude of node 3 in Figure 5e lies at the margin of machine precision. In Figure 6, we show how both the amplitude, a_3, of the opposite core and the deviations, $\phi_n - n\phi$, of the phases are suppressed as ϕ varies; the cusps at $\phi = \pi/6$ provides further numerical evidence for complete suppression. Figure 6c shows that this suppression at $\phi = \pi/N$ persists for larger values of N. In particular, there is a droproff of approximately 15 orders of magnitude between the amplitude $a_{N/2-1}$ and the amplitude $a_{N/2}$ of the opposite core. For all four values of N, the amplitude of the opposite core lies at the margin of machine precision. These results do not depend on the number of Fourier nodes in the temporal discretization.

Finally, we compute the error in the asymptotic formulae for the amplitudes, a_n, and phases, θ_n. In Figure 7a, we plots the log of the L^2 error $\|a_n^{\text{num}} - a_n^{\text{asymp}}\|_{L^2}$ vs. the log of coupling parameter k, where a_n^{num} is obtained from numerical parameter continuation, a_n^{asymp} is computed using (14),

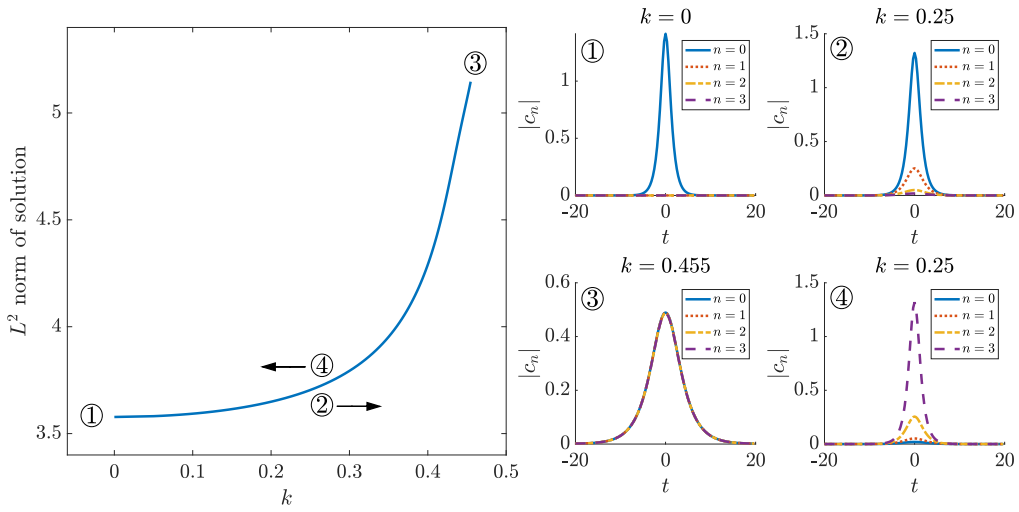

FIGURE 3. Parameter continuation in k for solutions to (5) for $\phi = 0.25$. Left panel: Continuation diagram plotting L^2 norm of entire solution vs. k. Right panels: Amplitudes at the first four sites of representative solutions, which correspond to labeled points on the continuation diagram. Label 2 is at $k = 0.25$ in the direction of increasing k. Label 4 is at $k = 0.25$ in the direction of decreasing k. 128 Fourier nodes per core.

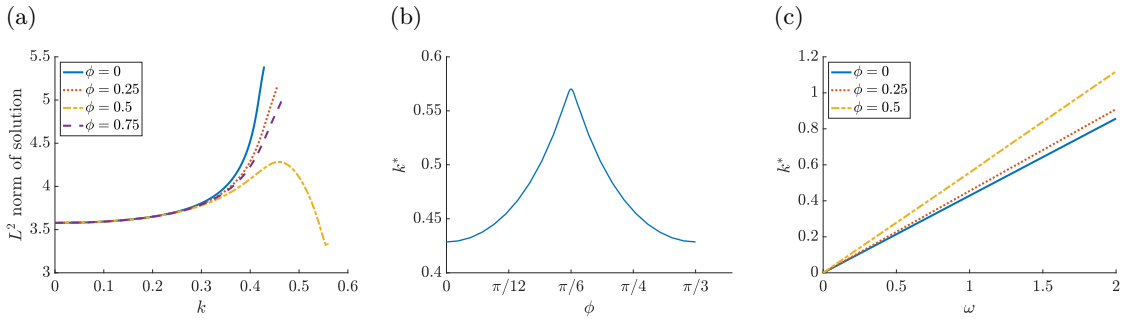

FIGURE 4. Parameter continuation in k for solutions to (5). (a) Continuation diagram plotting L^2 norm of entire solution vs. k for various ϕ. (b) Plot of critical value k^* vs. ϕ for $\omega = 1$. (c) Plot of critical value k^* vs ω for various ϕ. 128 Fourier nodes per core.

(17), and (16), and the L^2 norm on the periodic domain $[-T, T]$ is defined by

$$\|f\|_{L^2} = \int_{-T}^{T} |f(t)|^2 dt.$$

The slopes of least squares regressions lines for the error in a_0, a_1, a_2, and a_3 are within 5% of 4, 3, 4, and 5 (respectively). For $n \geq 1$, this agrees with the order of the remainder term for a_n in (14). The order of the remainder term for a_0 is one order higher in k than in (14). For $k \leq 0.2$, the relative L^2 error

$$\frac{\|a_n^{\text{num}} - a_n^{\text{asymp}}\|_{L^2}}{|a_n^{\text{num}}\|_{L^2}}$$

is less than 0.05.

Since the formulas (19) involve the products, $a_n\theta_n$, of the amplitudes and phases, Figure 7b plots the log of the L^2 error of $\|(a_n(\theta_n - n\phi)^{\text{num}} - a_n(\theta_n - n\phi)^{\text{asymp}}\|_{L^2}$ vs. the log of coupling parameter k, where the true value is obtained from numerical parameter continuation, and the approximate value is computed using $a_n(\theta_n - n\phi)^{\text{asymp}} = k^{N-n}\widetilde{a}_n\widetilde{\theta}_n$ and (19). The slopes of least squares regressions lines for the error in $a_1\theta_1$ and $a_2\theta_2$ are within 2.5% of 5 and 4 (respectively),

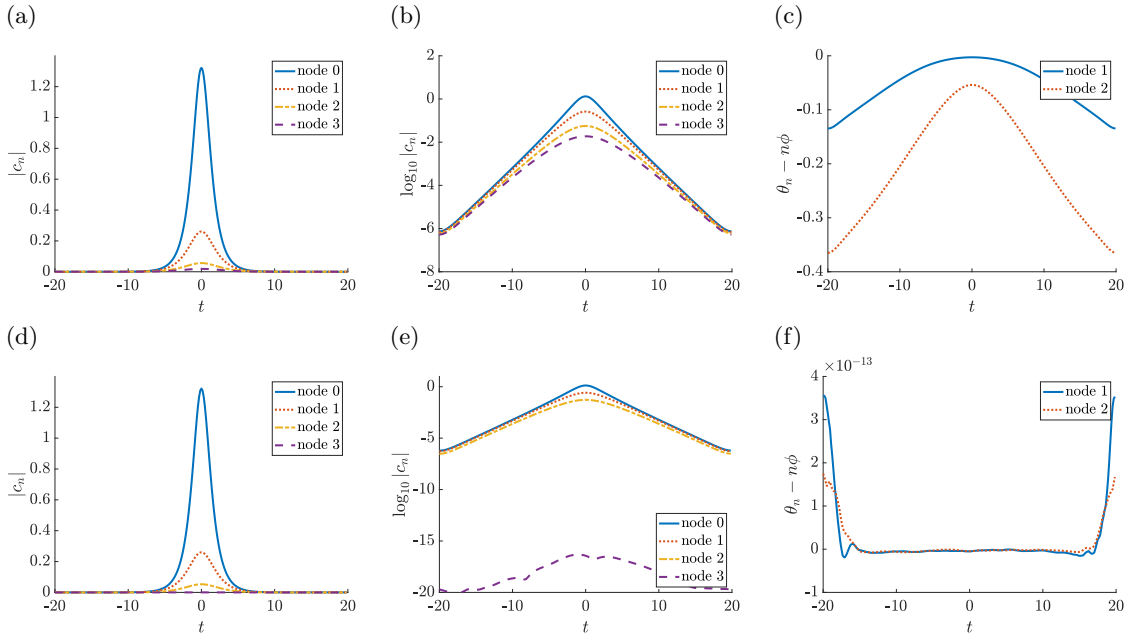

FIGURE 5. Spatiotemporal solutions to equation (5) for $N = 6$ waveguides and $k = 0.25$. The twist parameter is $\phi = 0.25$ (top) and $\phi = \pi/6$ (bottom). Left and middle: Amplitude and log amplitude of solution at first four sites. Right: $\theta_n(t) - n\phi$ for sites 1 and 2.

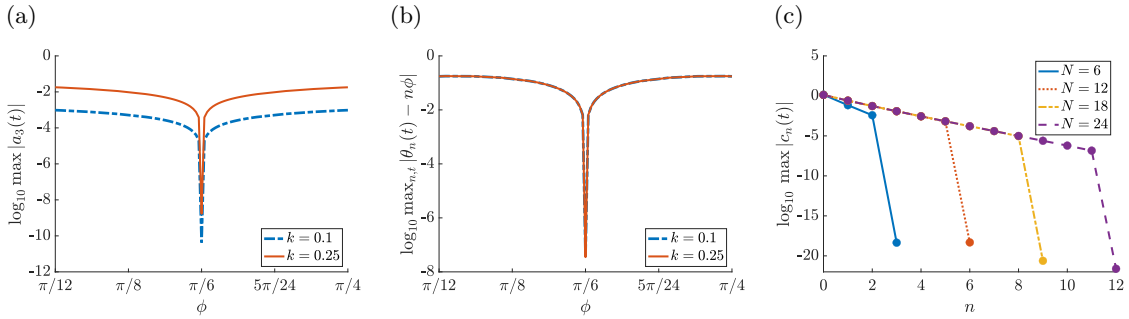

FIGURE 6. (a) $\log_{10}\max|a_3(t)|$ vs. ϕ for $k = 0.1$ and $k = 0.25$. (b) $\log_{10}\max_{n,t}|\theta_n(t) - n\phi|$ vs. ϕ for $k = 0.1$ and $k = 0.25$. (c) $\log_{10}\max|c_n(t)|$ vs. lattice site n for varying N, with twist parameter $\phi = \pi/N$, $k = 0.25$, and 128 Fourier nodes.

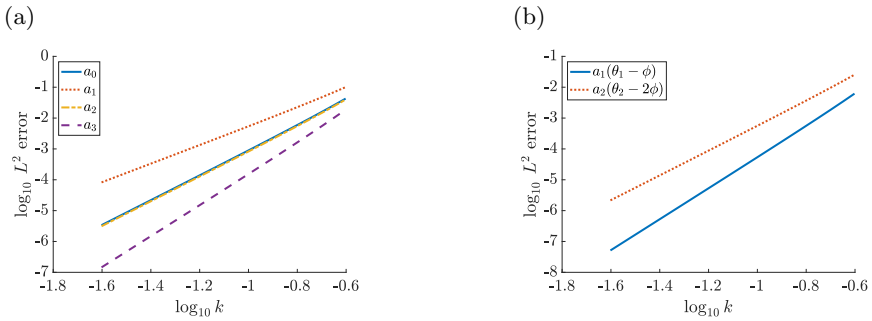

FIGURE 7. (a) $\log_{10}$ of L^2 error of the amplitudes a_n vs $\log_{10} k$, and (b) the product of the amplitudes and phases $a_n\theta_n$ vs $\log_{10} k$. (We note that $0.25 \approx 10^{-0.6}$).

which suggests that the order of the remainder term in k is correct in the asymptotic expansions (14) for θ_n.

5. Stability

To analyze the stability of a solution to (6), we express each c_n as $c_n = u_n + iv_n$, and let $c = (u_1, \dots, u_n, v_1, \dots, v_n) \in \mathbb{R}^{2N}$. The linearization of the PDE (3) about the pulse, c, is the linear operator $\mathcal{L}(c)$ on $H^2(\mathbb{R}, \mathbb{R}^{2N}) \subset L^2(\mathbb{R}, \mathbb{R}^{2N})$, defined by

$$\mathcal{L}(c) = \begin{pmatrix} kA_s(\phi) + 2\operatorname{diag}(u_n v_n) & \partial_t^2 - \omega + kA_c(\phi) + \operatorname{diag}(u_n^2) + 3\operatorname{diag}(v_n^2) \\ -\partial_t^2 + \omega - kA_c(\phi) - 3\operatorname{diag}(u_n^2) - \operatorname{diag}(v_n^2) & kA_s(\phi) - 2\operatorname{diag}(u_n v_n) \end{pmatrix}, \tag{24}$$

where $A_c(\phi)$ and $A_s(\phi)$ are defined in (22) and (23). The spectrum of $\mathcal{L}(c)$ is the union of the essential spectrum and the point spectrum. Since the pulse is even in the spatial variable, the essential spectrum is the set of $\lambda \in \mathbb{C}$ for which $\mathcal{L}(c) - \lambda\mathcal{I}$ is not Fredholm [8, Section 3.1]. The point spectrum is the set of $\lambda \in \mathbb{C}$ for which $\ker(\mathcal{L}(c) - \lambda\mathcal{I})$ is nontrivial. The essential spectrum depends only on the background state, i.e. is independent of c. Since the operator $\mathcal{L}(c)$ is exponentially asymptotic to the linear operator $\mathcal{L}(0)$, given by

$$\mathcal{L}(0) = \begin{pmatrix} kA_s(\phi) & \partial_t^2 - \omega + kA_c(\phi) \\ -\partial_t^2 + \omega - kA_c(\phi) & kA_s(\phi) \end{pmatrix}, \tag{25}$$

it follows from the Weyl essential spectrum theorem [8, Theorem 2.2.6] that the essential spectrum of $\mathcal{L}(c)$ is given by the essential spectrum of the constant coefficient operator $\mathcal{L}(0)$, which we compute in appendix C. Consequently, we obtain the following result.

Proposition 1. *For $0 \le \phi \le \frac{2\pi}{N}$, define α in terms of ϕ by*

$$\alpha = \begin{cases} \omega - 2k\cos(\phi), & 0 \le \phi \le \frac{\pi}{N}, \\ \omega - 2k\cos\left(\frac{2\pi}{N} - \phi\right), & \frac{\pi}{N} \le \phi \le \frac{2\pi}{N}, \end{cases} \tag{26}$$

and extend α periodically in ϕ with period $2\pi/N$. If ω, k, and ϕ are chosen so that $\alpha > 0$, the essential spectrum comprises two symmetric, disjoint bands on the imaginary axis

$$\sigma_{ess} = i(-\infty, -\alpha] \cup i[\alpha, \infty), \tag{27}$$

and α attains a maximum of $\omega - 2k\cos(\pi/N)$ when $\phi = \pi/N$.

We note that the essential spectrum is bounded away from the origin when $\alpha > 0$. In addition, both α and k^* attain a maximum at $\phi = \pi/N$.

The spectrum of $\mathcal{L}(c)$ can be numerically approximated by discretizing the differentiation matrices in (24) using Fourier spectral differentiation matrices, writing the operator as a block matrix, and computing the eigenvalues of that matrix using MATLAB's eigenvalue solver `eig`. The two essential spectrum bands can be seen in the top row of Figure 8. Due to the spatial discretization, the continuous bands constituting the essential spectrum are approximated by discrete sets of points. In Figure 8c, we plot the border, α, of the essential spectrum as a function of the coupling parameter, k. The results obtained using the matrix discretization of the operator are shown with the red dashed curve, and those obtained using (26) are shown with the yellow dotted curve. The relative error of the numerical result is less than 1%.

We now turn to the point spectrum of $\mathcal{L}(c)$. As for the NLS equation [9, Chapter 2.1.1.1], the kernel of $\mathcal{L}(c)$ has algebraic multiplicity 4 and geometric multiplicity 2. The kernel is spanned by the two eigenfunctions $w_1 = (\partial_t u_1, \dots, \partial_t u_N, \partial_t v_1, \dots, \partial_t v_N)^T$ and $w_2 = (-v_1, \dots, -v_N, u_1, \dots, u_N)^T$. In addition, there is a pair of internal mode eigenvalues $\pm\lambda_e$, which will call edge modes since they split off from the edge of the essential spectrum (these can be seen in Figure 8a). As k increases, λ_e moves towards the origin (see Figure 8c for a plot of λ_e vs. k), collides with the eigenvalues at the origin at a critical value $k = k_e$, and then moves onto the real axis (Figure 8b). This suggests that the solution c is neutrally stable for $0 < k < k_e$ and unstable for $k > k_e$. A plot of this critical value k_e vs. ϕ in Figure 8d suggests that the maximum value of k_e occurs when $\phi = \pi/N$.

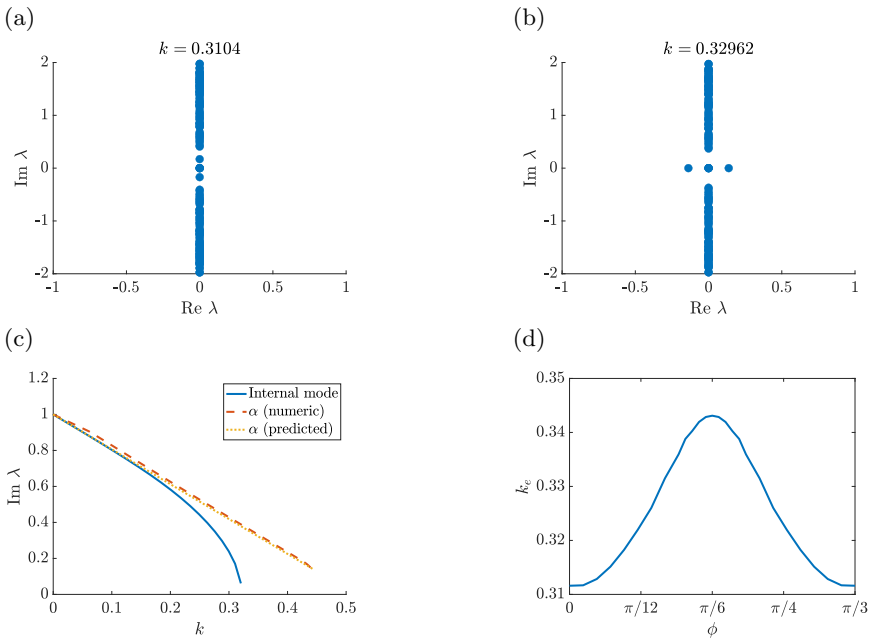

FIGURE 8. (a), (b) Spectrum of $\mathcal{L}(c)$ before and after collision of internal mode eigenvalue with origin. (c) Plot of predicted essential spectrum border α, computed essential spectrum border, and internal mode eigenvalue vs. k. (d) Plot of critical value k_e for internal mode eigenvalue collision vs. ϕ. The twist parameter is $\phi = 0.25$ for all plots.

Numerical evolution experiments using MATLAB's `ode45` function suggest that this internal mode primarily affects the phases, θ_n, of the pulses. For $k < k_e$, the internal mode eigenvalue, λ_e, is imaginary. Evolution of perturbations in the direction of the corresponding eigenmode v_e exhibits phase oscillations with frequency, λ_e, with relative error less than 10^{-3} (see Figure 9b). For $k > k_e$, the internal mode eigenvalue, λ_e, is real. Evolution of perturbations in the direction of the corresponding eigenmode, v_e, exhibits exponential growth in the phases; the growth rate is λ_e with relative error less than 10^{-2} (see Figure 9d). We note that in both cases, the amplitudes of the perturbed solutions also exhibit oscillatory behavior (Figure 9a and Figure 9c), although the magnitude of these oscillations in L^2 norm is much larger for $k > k_e$ than for $k < k_e$.

6. Conclusions

In this paper, we studied a model of light propagation in a twisted multi-core fiber that includes temporal dispersion. We derived asymptotic expressions for spatiotemporal solutions in which the number of waveguides, N, is even, the bulk of the intensity is contained in a single node (the primary core), and the amplitudes and phases of the solution obey certain symmetry relations. This asymptotic analysis is valid for arbitrary, even N. These expressions are in very good agreement with results from numerical parameter continuation. Furthermore, the asymptotic analysis shows that for an even number, N, of waveguides, there is significant suppression of optical activity in the waveguide opposite the primary core when the twist parameter, ϕ, and the number of waveguides, N, are related by $\phi = \pi/N$. This is the exact same behavior found in the model with no temporal dispersion [17]. Numerical computation suggests that there are two critical values, k_e and k^*, of k, with $0 < k_e < k^*$. The pulse solution exists for $0 < k < k^*$ and is stable for $0 < k < k_e$, at which point an internal eigenmode collides with the eigenvalues at the origin. Both k_e and k^* attain their maximum when $\phi = \pi/N$, which is also the angle for which the essential spectrum boundary, α, is furthest from the origin.

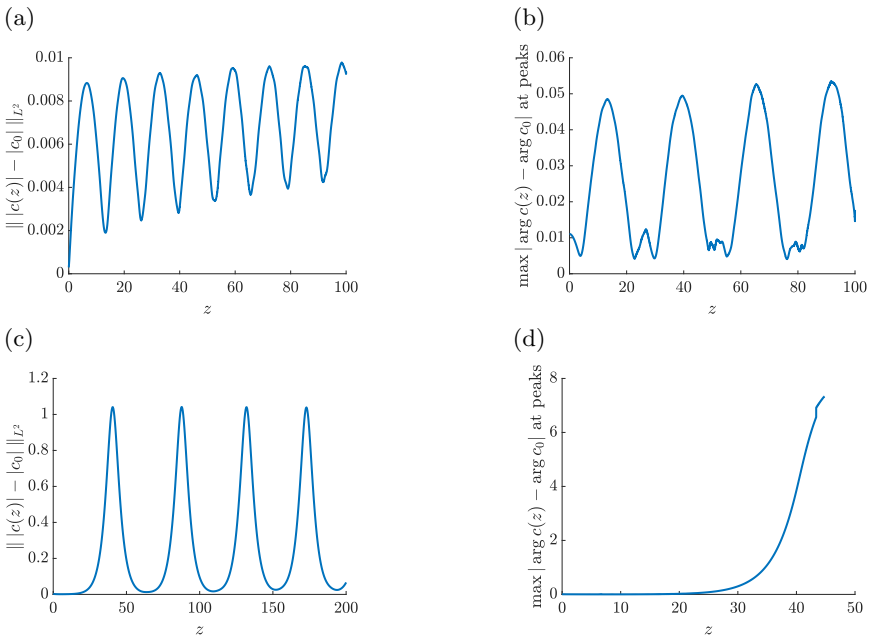

FIGURE 9. Evolution, $c(z)$, in z of perturbations of the pulse solution, c_0, for $k = 0.25$ (top, edge mode $\lambda = \pm 0.239i$) and $k = 0.35$ (bottom, edge mode $\lambda = \pm 0.255$). The initial condition is $c_0 + \epsilon v_e$, where v_e is the eigenfunction corresponding to the edge mode and $\epsilon = 10^{-2}$. Left panels: Evolution of the L^2 norm difference between the amplitude $|c(z)|$ of perturbation and the amplitude $|c_0|$ of the pulse. Right panels: Evolution of phase differences at centers of peaks between the perturbation $c(z)$ and the pulse c_0. Twist parameter $\phi = 0.25$ for all plots.

Future research could include exploring the case with odd N, which was considered in the model without temporal dispersion. As in [17], this would involve a different set of symmetries, and it may be possible that a configuration could be found in which there would be optical suppression of a single site when $\phi = \pi/N$. Furthermore, we only considered solutions which obey the symmetries (12). Solution branches with these symmetries cease to exist for $k > k^*$, where k^* is the point at which all cores have attained equal amplitudes. It is possible that there exist asymmetric solutions for which $k > k^*$. We could also study multi-pulses, which are solutions in which the energy is concentrated at multiple sites in the ring. These have been well-studied in DNLS [18], and we considered them briefly in [17]. Finally, if the distances between neighboring waveguides are small, nonlocal interactions might become significant, suggesting a model with coupling that extends beyond nearest neighbors. We could, for example, incorporate next-to-next-nearest neighbor interactions, as was done with DNLS in [24].

It could also be interesting to extend the model to more complicated geometries, such as twisted optical fibers comprising multiple concentric rings, or to study the evolution of these solutions in the presence of imperfections in the fiber. Another avenue of exploration would be to examine the continuum limit, i.e. what happens as $N \to \infty$. Since the fiber radius R is held constant, the ring becomes more "densely" packed with waveguides as N increases, and in the limit as $N \to \infty$, this becomes a continuum on the circle of radius R. Furthermore, the twist parameter, ϕ, is proportional to $1/N$, and so $\phi \to 0$ as $N \to \infty$. An interesting question is to what extent the twist is preserved in the equations for the continuum limit. Finally, since these solutions are stable for $k < k_e$, it would be interesting compare these results with experimental realizations.

Acknowledgments: This material is based upon work supported by the U.S. National Science Foundation under the RTG grant DMS-1840260 (R.P. and A.A.), DMS-1909559 (A.A.), and DMS-2106203 (J.Z.).

Appendix A. Symmetries

We verify that the symmetry relations in (12) are consistent with (9), i.e. solutions to (9) can exist with these symmetries. First, for $n = 2, \dots, N/2-1$, we take equation (9) for $-n$, substitute the symmetries for a_n and θ_n from (12), and simplify, to obtain

$$\begin{aligned}&(\ddot{a}_n - a_n(\dot{\theta}_n)^2) - i(a_n\ddot{\theta}_n + 2\dot{a}_n\dot{\theta}_n)\\ &\quad + k\left(a_{n-1}e^{i[(\theta_n-\theta_{n-1})-\phi]} + a_{n+1}e^{-i[(\theta_{n+1}-\theta_n)-\phi]}\right) + a_n^3 - \omega a_n = 0,\end{aligned}$$

which is the complex conjugate of (9) for n. For $n = 0$, we take equation (9) for $n = 0$, substitute the symmetries for a_n and θ_n from (12), and simplify, to obtain

$$(\ddot{a}_0 - a_0(\dot{\theta}_0)^2) + i(a_0\ddot{\theta}_0 + 2\dot{a}_0\dot{\theta}_0) + 2ka_1\cos(\theta_1-\phi)(\cos\theta_0 + i\sin\theta_0) + a_n^3 - \omega a_n = 0.$$

The imaginary part is

$$a_0\ddot{\theta}_0 + 2\dot{a}_0\dot{\theta}_0 = 2ka_1\cos(\theta_1-\phi)\sin\theta_0, \tag{28}$$

for which $\theta_0 = 0$ is a solution, thus this condition is consistent. Following the same procedure by using the imaginary part of equation (9), we can show that the $\theta_{N/2} = 0$ is a solution to the imaginary part of (9) for $n = N/2$, thus this condition is consistent as well.

Appendix B. Asymptotic analysis

Let a_n and θ_n be the amplitudes and phases at site n, as in the ansatz (8), where $n \in S = \{0, \pm1, \dots, \pm N/2-1, N/2\}$. We assume that

$$a_n, \theta_n \in H^2(\mathbb{R}) \subset L^2(\mathbb{R}),$$

where $L^2(\mathbb{R})$ is the space of real, valued square-integrable functions on $\mathbb{R}$ equipped with the standard inner product, and $H^2(\mathbb{R})$ is the corresponding Sobolev space. We note that the system of equations (9) is translation invariant, i.e. if $\{a_n(t), \theta_n(t)\}_{n\in S}$ is a solution, then so is $\{a_n(t-\tau), \theta_n(t-\tau)\}_{n\in S}$ for any $\tau \in \mathbb{R}$. When $k = 0$, we want the solution a_0 to be the ordinary NLS soliton ψ, which is centered at 0. To ensure that the solution we find is not shifted in t, we impose the phase condition,

$$\langle a_0, \dot{\psi}\rangle_{L^2(\mathbb{R})} = \int_{-\infty}^{\infty} a_0(t)\dot{\psi}(t)dt = 0, \tag{29}$$

on the amplitude a_0. In other words, a_0 has no component in the direction of $\dot{\psi}$.

We define the linear operator $\mathcal{L}_\omega : H^2(\mathbb{R}) \subset L^2(\mathbb{R}) \to L^2(\mathbb{R})$ by

$$\mathcal{L}_\omega = \omega - \partial_t^2. \tag{30}$$

The kernel of $\mathcal{L}_\omega$ is $\{0\}$, i.e. the only solution in $H^2(\mathbb{R})$ to $\mathcal{L}_\omega f = 0$ is $f = 0$, which can be verified by taking the Fourier transform of $\mathcal{L}_\omega$. Consequently, the operator $\mathcal{L}_\omega$ is invertible on $L^2(\mathbb{R})$. We also note that if we use periodic boundary conditions on $[-T, T]$, as long as we take $\omega > 0$, $\ker\mathcal{L}_\omega = \{0\}$, and $\mathcal{L}_\omega$ is invertible on $L^2_{\text{per}}([-T, T])$.

Next, we recall that the NLS soliton, ψ, is a real-valued, standing wave solution to the NLS equation with frequency ω, thus it solves

$$\ddot{u} + u^3 - \omega u = 0. \tag{31}$$

Linearizing this equation about ψ yields the self-adjoint linear operator $\mathcal{L}(\psi) : H^2(\mathbb{R}) \subset L^2(\mathbb{R}) \to L^2(\mathbb{R})$, defined by

$$\mathcal{L}(\psi) = \partial_t^2 - \omega + 3\psi^2. \tag{32}$$

The kernel of $\mathcal{L}(\psi)$ is one-dimensional, and is spanned by $\dot{\psi}$. By the Fredholm alternative [26], since $\mathcal{L}(\psi)$ is self-adjoint, the equation $\mathcal{L}(\psi) = u$ has a solution if $u \perp \dot{\psi}$.

B.1. **Primary core.** Using the symmetry relations (12) and $\theta_0 = 0$, equation (10) for $n = 0$ becomes

$$\ddot{a}_0 + 2ka_1 \cos(\theta_1 - \phi) + a_0^3 - \omega a_0 = 0. \tag{33}$$

We take the power series ansatz

$$a_0 = \psi + ka_0^{(1)} + k^2 a_0^{(2)} + \mathcal{O}(k^3)$$

for the amplitude a_0, where ψ is the NLS soliton (7). In addition, from (13), we have, at minimum,

$$a_1 = k\widetilde{a}_1 + \mathcal{O}(k^2), \qquad \theta_1 = \phi + \mathcal{O}(k).$$

Substituting this into (33), using the Taylor series expansion $\cos(\theta_1 - \phi) = \mathcal{O}(k^2)$, collecting powers of k, and simplifying, we obtain

$$\begin{aligned}\left(\ddot{\psi} + \psi^3 - \omega\psi\right) + k\left(\ddot{a}_0^{(1)} - \omega a_0^{(1)} + 3\psi^2 a_0^{(1)}\right) \\ + k^2\left(\ddot{a}_0^{(2)} - \omega a_0^{(2)} + 3\left(a_0^{(1)}\right)^2 + 3\psi^2 a_0^{(2)} + 2\widetilde{a}_1\right) + \mathcal{O}(k^3) = 0.\end{aligned}$$

The $\mathcal{O}(1)$ term is 0 since ψ solves (31). The $\mathcal{O}(k)$ term can be written as $\mathcal{L}(\psi)a_0^{(1)} = 0$, where $\mathcal{L}(\psi)$ is defined by (32). Since the kernel of $\mathcal{L}(\psi)$ is spanned by $\dot{\psi}$, $a_0^{(1)} = c\dot{\psi}$ for some constant c. However, since we wish our solution to satisfy the phase condition (29), we require that $a_0^{(1)} = 0$. The $\mathcal{O}(k^2)$ term then becomes

$$\ddot{a}_0^{(2)} - \omega a_0^{(2)} + 3\psi^2 a_0^{(2)} + 2\widetilde{a}_1 = 0.$$

Letting $\widetilde{a}_0 = a_0^{(2)}$, we rewrite this as

$$\mathcal{L}(\psi)\widetilde{a}_0 = -2\widetilde{a}_1, \tag{34}$$

which is the first equality in (16). Once we determine $\widetilde{a}_1$, which we will do in the next step, we can solve for $\widetilde{a}_0$, provided $\widetilde{a}_1 \perp \dot{\psi}$. Putting all of this together, we have the expression for a_0

$$a_0 = \psi + k^2\widetilde{a}_0 + \mathcal{O}(k^3) = \psi + \mathcal{O}(k^2), \tag{35}$$

which is the first equation in (14).

B.2. **Amplitudes.** We can now determine the leading order terms for the amplitudes a_n, for $n = 1, \ldots, N/2$, using the real parts (10) of the equations (9). The phases θ_n will be determined in the next step. For $n = 1$, we take the power series ansatz

$$a_1 = k\widetilde{a}_1 + \mathcal{O}(k^2).$$

From (13), we have, at minimum,

$$a_2 = \mathcal{O}(k^2), \qquad \theta_1 = \phi + \mathcal{O}(k), \qquad \theta_2 = 2\phi + \mathcal{O}(k),$$

and we note that $\dot{\theta}_1 = \mathcal{O}(k)$. Substituting these together with the expression (35) for a_0 into the $n = 1$ equation of (10), expanding the cosine terms in Taylor series, collecting powers of k, and simplifying, we obtain the equation

$$k\left(\partial_t^2\widetilde{a}_1 - \omega\widetilde{a}_1 + \psi\right) + \mathcal{O}(k^2) = 0.$$

We note that the nonlinear term a_1^3 does not contribute to the lowest order term in the asymptotic expansion. We use the $\mathcal{O}(k)$ term to solve for $\widetilde{a}_1$ to obtain

$$\widetilde{a}_1 = (\omega - \partial_t^2)^{-1}\psi, \tag{36}$$

which has a solution since $\mathcal{L}_\omega$ is invertible. This is the first equation in (15). Therefore,

$$a_1 = k(\omega - \partial_t^2)\psi + \mathcal{O}(k^2). \tag{37}$$

We continue this process iteratively from $n = 2$ to $n = N/2 - 1$. We take the power series ansatz

$$a_n = k^n \widetilde{a}_n + \mathcal{O}(k^{n+1}),$$

and use

$$\begin{aligned} a_{n-1} &= k^{n-1}\widetilde{a}_{n-1} + \mathcal{O}(k^n), & a_{n+1} &= \mathcal{O}(k^{n+1}), \\ \theta_{n-1} &= (n-1)\phi + \mathcal{O}(k), & \theta_{n+1} &= (n+1)\phi + \mathcal{O}(k), \end{aligned}$$

where the expression for a_{n-1} was found in the previous step. Substituting these into (10) and following the same procedure as above, we obtain the equation

$$k^n \left(\partial_t^2 \widetilde{a}_n - \omega \widetilde{a}_n + \widetilde{a}_{n-1}\right) + \mathcal{O}(k^{n+1}) = 0.$$

We use the $\mathcal{O}(k^n)$ term to solve for $\widetilde{a}_n$ to obtain

$$\widetilde{a}_n = (\omega - \partial_t^2)^{-1}\widetilde{a}_{n-1}, \tag{38}$$

which is the second equation in (15). This gives us

$$a_n = k^n(\omega - \partial_t^2)^{-1}\widetilde{a}_{n-1} + \mathcal{O}(k^{n+1}). \tag{39}$$

We will show in appendix B.4 that the remainder term is $\mathcal{O}(k^{n+2})$.

For the opposite core, $n = N/2$, we take $\theta_{N/2} = 0$ in the real part of (9) for $n = N/2$, use the symmetry relations for $a_{N/2-1}$ and $\theta_{N/2-1}$ from (12), and simplify to obtain

$$\ddot{a}_{N/2} - a_{N/2}(\dot{\theta}_{N/2})^2 + 2k a_{N/2-1}\cos(\theta_{N/2-1} + \phi) + a_{N/2}^3 - \omega a_{N/2} = 0. \tag{40}$$

Using the power series ansatz

$$a_{N/2} = k^{N/2}\widetilde{a}_{N/2} + \mathcal{O}(k^{N/2+1})$$

and the formula $a_{N/2-1} = k^{N/2-1}\widetilde{a}_{N/2-1} + \mathcal{O}(k^{N/2})$ from the previous step, we obtain the expression

$$\widetilde{a}_{N/2} = 2(\omega - \partial_t^2)^{-1}\cos(\theta_{N/2-1} + \phi)\widetilde{a}_{N/2-1}. \tag{41}$$

It is important to note that since $\theta_{N/2} = 0$, the cosine term in (41) is order $\mathcal{O}(1)$. Substituting the ansatz $\theta_{N/2-1} = (N/2-1)\phi + \mathcal{O}(k)$ and simplifying, equation (41) becomes

$$\widetilde{a}_{N/2} = 2\cos(N\phi/2)(\omega - \partial_t^2)^{-1}\widetilde{a}_{N/2-1} + \mathcal{O}(k), \tag{42}$$

which is the third equation in (15). Since $\widetilde{a}_{N/2} = \mathcal{O}(1)$, it follows that

$$a_{N/2} = 2k^{N/2}\cos\left(N\phi/2\right)(\omega - \partial_t^2)^{-1}\widetilde{a}_{n-1} + \mathcal{O}(k^{N/2+1}). \tag{43}$$

Finally, since we have derived an expression (36) for $\widetilde{a}_1$, we substitute this into (34) to obtain

$$\mathcal{L}(\psi)\widetilde{a}_0 = -2(\omega - \partial_t^2)^{-1}\psi,$$

which we can solve for $\widetilde{a}_0$. This is the second equality in (16).

B.3. **Phases.** Now that we have determined the leading order terms for the amplitudes, a_n, we will compute the leading order terms for the phases, θ_n. In fact, we will get expressions for the products $\widetilde{a}_n\widetilde{\theta}_n$ of the leading order terms of the amplitudes and the phases. To do this, we will use the imaginary parts (11) of the equations (9), this time working backwards from $n = N/2 - 1$ to $n = 1$. (Equations (9) have already been satisfied for $n = N/2$ and $n = 0$ by taking $\theta_{N/2} = 0$ and $\theta_0 = 0$, respectively). For $n = N/2 - 1$, substitute the power series ansatz

$$\theta_{N/2-1} = k^2\widetilde{\theta}_{N/2-1} + \mathcal{O}(k^3),$$

the expressions for a_n from the previous section, $\theta_{N/2} = 0$, and $\theta_{N/2-2} = (N/2-2)\phi + \mathcal{O}(k^4)$ from (13) into equation (9) for $n = N/2 - 1$ to obtain

$$k^{N/2+1}\left(\widetilde{a}_{N/2-1}\ddot{\widetilde{\theta}}_{N/2-1} + 2\dot{\widetilde{a}}_{N/2-1}\dot{\widetilde{\theta}}_{N/2-1} - \widetilde{a}_{N/2-2}\widetilde{\theta}_{N/2-1} - \widetilde{a}_{N/2}\sin(N\phi/2)\right) + \mathcal{O}(k^{N/2+2}) = 0.$$

We use the $\mathcal{O}(k^{N/2+1})$ term to solve for $\widetilde{\theta}_{N/2-1}$. First, we solve equation (38) for $\widetilde{a}_{N/2-2}$ and substitute this above to obtain

$$\widetilde{a}_{N/2-1}\ddot{\widetilde{\theta}}_{N/2-1} + 2\dot{\widetilde{a}}_{N/2-1}\dot{\widetilde{\theta}}_{N/2-1} - \widetilde{\theta}_{N/2-1}(\omega - \partial_t^2)\widetilde{a}_{N/2-1} - \widetilde{a}_{N/2}\sin(N\phi/2) = 0,$$

which simplifies as the derivative of a product to obtain

$$(\omega - \partial_t^2)\left(\widetilde{a}_{N/2-1}\widetilde{\theta}_{N/2-1}\right) = -\sin(N\phi/2)\widetilde{a}_{N/2}.$$

Applying $(\omega - \partial_t^2)^{-1}$ to both sides, we obtain the formula

$$\widetilde{a}_{N/2-1}\widetilde{\theta}_{N/2-1} = -\sin(N\phi/2)(\omega - \partial_t^2)^{-1}\widetilde{a}_{N/2}, \tag{44}$$

and we can divide by $\widetilde{a}_{N/2-1}$ to solve for $\widetilde{\theta}_{N/2-1}$. Using equation (42) for $\widetilde{a}_{N/2}$, equation (44) becomes

$$\widetilde{a}_{N/2-1}\widetilde{\theta}_{N/2-1} = -2\sin(N\phi/2)\cos(N\phi/2)(\omega - \partial_t^2)^{-2}\widetilde{a}_{N/2-1},$$

which simplifies to

$$\widetilde{a}_{N/2-1}\widetilde{\theta}_{N/2-1} = -\sin(N\phi)(\omega - \partial_t^2)^{-2}\widetilde{a}_{N/2-1}, \tag{45}$$

using the double angle formula. This is the first equation in (18).

We now follow an iterative procedure from $n = N/2 - 2$ down to $n = 1$. For n, substitute the power series ansatz

$$\theta_n = k^{N-2n}\widetilde{\theta}_n + \mathcal{O}(k^{N-2n+1}),$$

the expressions for a_n from the previous section, and θ_n from (13) into equation (11) for n, and simplify, to obtain

$$k^{N/2}\left(\widetilde{a}_n\ddot{\widetilde{\theta}}_n + 2\dot{\widetilde{a}}_n\dot{\widetilde{\theta}}_n - \widetilde{a}_{n-1}\widetilde{\theta}_n + \widetilde{a}_{n+1}\widetilde{\theta}_{n+1}\right) + \mathcal{O}\left(k^{N/2+1}\right) = 0.$$

We use the $\mathcal{O}(k^{N/2})$ term to solve for $\widetilde{\theta}_n$. First, we solve equation (38) for $\widetilde{a}_{n-1}$ and substitute this above to obtain

$$\widetilde{a}_n\ddot{\widetilde{\theta}}_n + 2\dot{\widetilde{a}}_n\dot{\widetilde{\theta}}_n - \widetilde{\theta}_n(\omega - \partial_t^2)\widetilde{a}_n + \widetilde{a}_{n+1}\widetilde{\theta}_{n+1} = 0,$$

which simplifies as the derivative of a product to obtain

$$(\omega - \partial_t^2)\left(\widetilde{a}_n\widetilde{\theta}_n\right) = \widetilde{a}_{n+1}\widetilde{\theta}_{n+1}.$$

Applying $(\omega - \partial_t^2)^{-1}$ to both sides, we obtain the formula

$$\widetilde{a}_n\widetilde{\theta}_n = (\omega - \partial_t^2)^{-1}\left(\widetilde{a}_{n+1}\widetilde{\theta}_{n+1}\right), \tag{46}$$

which is the second equation in (18). We can divide by $\widetilde{a}_n$ to solve for $\widetilde{\theta}_n$.

B.4. **Higher order terms.** We briefly consider the higher order terms in the asymptotic expansion for the amplitudes, a_n. This will give us estimates for the order of the remainder term in the asymptotic expansion for a_n which are slightly better than we obtained in appendix B.2. We also obtain an improved estimate for the remainder term in the opposite core when $\phi = \pi/N$. We take the asymptotic series ansatz

$$a_n = k^n \sum_{j=0}^{\infty} a_n^{(j)} k^j \qquad\qquad n = 0, \dots, \frac{N}{2}, \tag{47}$$

where, using the notation in the previous section for the leading order terms, we have $a_0^0 = \psi$, $a_0^1 = 0$, $a_0^2 = \tilde{a}_0$, and $a_n^0 = \tilde{a}_n$ for $n = 1, \dots, N/2$. Substituting this into (10), using the estimate in (13) for θ_n, and simplifying, we obtain the following expression for the next-to-leading order terms:

$$\begin{aligned} \mathcal{L}(\psi) a_0^{(3)} &= -2a_1^{(1)} \\ a_n^{(1)} &= (\omega - \partial_t^2)^{-1} a_{n-1}^{(1)} \qquad\qquad n = 1, \dots, N/2 - 1 \\ a_{N/2}^{(1)} &= 2\cos(N\phi/2)(\omega - \partial_t^2)^{-1} a_{N/2-1}^{(1)}. \end{aligned}$$

Since $a_0^{(1)} = 0$, $a_n^{(1)} = 0$ for $n = 1, \dots, N/2$, from which it follows that $a_n = k^n \widetilde{a}_n + \mathcal{O}(k^{n+2})$ for $n \geq 1$, which is the second equation in (14). In principle, we can continue this process to obtain still higher order correction terms, although we note that the expressions we obtain will become increasingly more unwieldy. The next term in the asymptotic series, for example, is

$$a_n^{(2)} = (\omega - \partial_t^2)^{-1}(a_{n-1}^{(2)} + a_{n+1}^0) \qquad\qquad n = 1, \dots, N/2 - 1,$$

which involves a contribution from both neighboring nodes. Higher terms in the series will incorporate contributions from the nonlinearity as well as the phase θ_n.

For the opposite core, we substitute the power series ansatz (47), $\theta_{N/2} = 0$, and the estimate $\theta_{N/2-1} = \mathcal{O}(k^2)$ from (18) into (40), expand the cosine term in a Taylor series, and simplify to obtain

$$\sum_{j=0}^{\infty} a_{N/2}^{(j)} k^j + 2\left[\cos(N\phi/2) + \mathcal{O}(k^4)\right] \sum_{j=0}^{\infty} a_{N/2-1}^{(j)} k^j - \omega \sum_{j=0}^{\infty} a_{N/2}^{(j)} + \mathcal{O}(k^N) = 0.$$

Since N is even, and we will always take $N \geq 4$, the $\mathcal{O}(k^4)$ terms will only contribute for $j \geq 4$, thus we obtain

$$a_{N/2}^{(j)} = 2\cos(N\phi/2)(\omega - \partial_t^2)^{-1} a_{N/2-1}^{(j)} \qquad\qquad j = 0, 1, 2, 3.$$

It follows that if $\phi = \pi/N$, $a_{N/2}^{(j)} = 0$ for $j = 0, 1, 2, 3$, in which case we obtain the estimate

$$a_{N/2} = \mathcal{O}\left(k^{N/2+4}\right).$$

Appendix C. Proof of Proposition 1

Following [8, Section 3.1] (see, in particular, Section 3.1.1.5, concerning the NLS equation), $\lambda \in \sigma_{\text{ess}}(\mathcal{L}(0))$ if and only if $\mathcal{L}(0) - \lambda$ has an imaginary spatial eigenvalue, i.e. $(\mathcal{L}(0) - \lambda\mathcal{I}) \begin{pmatrix} u \\ v \end{pmatrix} e^{irt}$ has a solution for $r \in \mathbb{R}$ and $u, v \in \mathbb{C}^N$. After simplification, this reduces to the system of equations

$$\begin{aligned} (kA_s - \lambda)u - (r^2 + \omega - kA_c)v &= 0 \\ (r^2 + \omega - kA_c)u + (kA_s - \lambda)v &= 0. \end{aligned} \tag{48}$$

A_c and A_s are both circulant matrices [6]. The eigenvalues, μ_j^c and μ_j^s, of the circulant matrices A_c and A_s, are given by

$$\mu_j^c = 2\cos\left(\frac{2\pi}{N}j\right)\cos\phi, \qquad \mu_j^s = 2i\sin\left(\frac{2\pi}{N}j\right)\sin\phi, \qquad j = 0,\dots,N-1, \tag{49}$$

and the corresponding common eigenvectors are given by

$$v_j = \frac{1}{\sqrt{N}}\left(1, \xi^j, \xi^{2j}, \dots, \xi^{(N-1)j}\right), \tag{50}$$

where $\xi = \exp\frac{2\pi i}{N}$ is a primitive Nth root of unity [6]. Since A_s and A_c appear in both equations in (48), we can only have a solution if u and v are scalar multiples of one of the eigenvectors v_j. Letting $u = b_1 v_j$ and $v = b_2 v_j$, the system of equations (48) reduces to

$$\begin{aligned}(k\mu_j^s - \lambda)b_1 - (r^2 + \omega - k\mu_j^c)b_2 &= 0\\ (r^2 + \omega - k\mu_j^c)b_1 + (k\mu_j^s - \lambda)b_2 &= 0,\end{aligned} \tag{51}$$

where we used the fact that $v_j \neq 0$. This has a nontrivial solution if and only if the determinant of the corresponding 2×2 coefficient matrix is 0, i.e.

$$(\lambda - k\mu_j^s)^2 + (r^2 + \omega - k\mu_j^c)^2 = 0.$$

For $k\mu_j^c \leq \omega$, this has a solution when

$$\begin{aligned}\lambda &= k\mu_j^s \pm i(r^2 + \omega - k\mu_j^c)\\ &= \pm i\left(r^2 + \omega \pm 2k\sin\left(\frac{2\pi}{N}j\right)\sin\phi - 2k\cos\left(\frac{2\pi}{N}j\right)\cos\phi\right)\\ &= \pm i\left(r^2 + \omega - 2k\cos\left(\frac{2\pi}{N}j \pm \phi\right)\right).\end{aligned}$$

As long as $2k\max_{j=0,\dots,N-1}\cos\left(\frac{2\pi}{N}j \pm \phi\right) \leq \omega$, $\lambda \in (-\infty, -\alpha]\cup[\alpha,\infty)$, where

$$\alpha = \omega - 2k\max_{j=0,\dots,N-1}\cos\left(\frac{2\pi}{N}\right). \tag{52}$$

For $0 \leq \phi \leq 2\pi/N$,

$$\alpha = \begin{cases}\omega - 2k\cos(\phi) & 0 \leq \phi \leq \frac{\pi}{N}\\ \omega - 2k\cos\left(\frac{2\pi}{N} - \phi\right) & \frac{\pi}{N} \leq \phi \leq \frac{2\pi}{N},\end{cases}$$

which has a maximum of $\omega - 2k\cos(\pi/N)$ when $\phi = \pi/N$. For ϕ outside of this interval, α is periodic with period $\frac{2\pi}{N}$.

References

1. Balakin A. A., S. A. Skobelev, A. V. Andrianov, E. A. Anashkina, and A. G. Litvak, *Coherent amplification of high-power laser radiation in multicore fibers from a rectangular array of cores*, Opt. Lett. **46** (2021), no. 2, 246–249.
2. Alejandro B. Aceves, Gregory G. Luther, Costantino De Angelis, Alexander M. Rubenchik, and Sergei K. Turitsyn, *Energy localization in nonlinear fiber arrays: Collapse-effect compressor*, Phys. Rev. Lett. **75** (1995), 73–76.
3. Serge Aubry and Gilles Abramovici, *Chaotic trajectories in the standard map. The concept of anti-integrability*, Physica D **43** (1990), 199–219.
4. Saeed Sharif Azadeh, Andrei Stalmashonak, Kevin W. Bennett, Fu-Der Chen, Wesley D. Sacher, and Joyce K. S. Poon, *Multicore fibers with 10 and 16 single-mode cores for the visible spectrum*, Opt. Lett. **47** (2022), no. 1, 26–29.
5. Claudia Castro-Castro, Yannan Shen, Gowri Srinivasan, Alejandro B. Aceves, and Panayotis G. Kevrekidis, *Light dynamics in nonlinear trimers and twisted multicore fibers*, J. Nonlinear Opt. Phys. Mater. **25** (2016), 1–11.

6. Philip Davis, *Circulant matrices*, AMS Chelsea Publishing, American Mathematical Society, Providence, Rhode Island, 2012.
7. Ivan L. Garanovich, Stefano Longhi, Andrey A. Sukhorukov, and Yuri S. Kivshar, *Light propagation and localization in modulated photonic lattices and waveguides*, Phys. Rep. **518** (2012), no. 1, 1–79.
8. Todd Kapitula and Keith Promislow, *Spectral and dynamical stability of nonlinear waves*, Springer New York, 2013.
9. Panayotis G. Kevrekidis, *The discrete nonlinear Schrödinger equation*, Springer Berlin Heidelberg, 2009.
10. Stefano Longhi, *Self-imaging and modulational instability in an array of periodically curved waveguides*, Opt. Lett. **30** (2005), 2137–2139.
11. ———, *Bloch dynamics of light waves in helical optical waveguide arrays*, Phys. Rev. B **76** (2007).
12. ———, *Light transfer control and diffraction management in circular fibre waveguide arrays*, J. Phys. B **40** (2007).
13. Daniel Loss, David P. DiVincenzo, and G. Grinstein, *Suppression of tunneling by interference in half-integer-spin particles*, Phys. Rev. Lett. **69** (1992), 3232–3235.
14. Stefano Minardi, Falk Eilenberger, Yaroslav V Kartashov, Alexander Szameit, Ulrich Röpke, Jens Kobelke, Key Schuster, Hartmut Bartelt, Stefan Nolte, Lluis Torner, et al., *Three-dimensional light bullets in arrays of waveguides*, Phys. Rev. Lett. **105** (2010), no. 26, 263901.
15. M. Ornigotti, G. Della Valle, D. Gatti, and S. Longhi, *Topological suppression of optical tunneling in a twisted annular fiber*, Phys. Rev. A **76** (2007), 023833.
16. Tomoki Ozawa, Hannah M Price, Alberto Amo, Nathan Goldman, Mohammad Hafezi, Ling Lu, Mikael C Rechtsman, David Schuster, Jonathan Simon, Oded Zilberberg, et al., *Topological photonics*, Rev. Mod. Phys. **91** (2019), no. 1, 015006.
17. Ross Parker and Alejandro Aceves, *Standing-wave solutions in twisted multicore fibers*, Phys. Rev. A **103** (2021), no. 5, 053505.
18. Ross Parker, P.G. Kevrekidis, and Björn Sandstede, *Existence and spectral stability of multi-pulses in discrete Hamiltonian lattice systems*, Physica D **408** (2020), 132414 (en).
19. Midya Parto, Helena Lopez-Aviles, Jose E. Antonio-Lopez, Mercedeh Khajavikhan, Rodrigo Amezcua-Correa, and Demetrios N. Christodoulides, *Observation of twist-induced geometric phases and inhibition of optical tunneling via Aharonov-Bohm effects*, Sci. Adv. **5** (2019), no. 1, 1–5.
20. Midya Parto, Helena Lopez-Aviles, Mercedeh Khajavikhan, Rodrigo Amezcua-Correa, and Demetrios N. Christodoulides, *Topological Aharonov-Bohm suppression of optical tunneling in twisted nonlinear multicore fibers*, Phys. Rev. A **96** (2017), 043816.
21. R. Peierls, *Zur Theorie des Diamagnetismus von Leitungselektronen*, Zeitschrift für Physik **80** (1933), no. 11-12, 763–791.
22. D.E. Pelinovsky, P.G. Kevrekidis, and D.J. Frantzeskakis, *Persistence and stability of discrete vortices in nonlinear Schrödinger lattices*, Physica D: Nonlinear Phenomena **212** (2005), no. 1-2, 20–53.
23. ———, *Stability of discrete solitons in nonlinear Schrödinger lattices*, Physica D: Nonlinear Phenomena **212** (2005), no. 1-2, 1–19.
24. T. Penati, M. Sansottera, S. Paleari, V. Koukouloyannis, and P.G. Kevrekidis, *On the nonexistence of degenerate phase-shift discrete solitons in a dNLS nonlocal lattice*, Physica D: Nonlinear Phenomena **370** (2018), 1–13.
25. Andrey Pryamikov, Ljupco Hadzievski, Mikhail Fedoruk, Sergei Turitsyn, and Alejandro Aceves, *Optical vortices in waveguides with discrete and continuous rotational symmetry*, J. Eur. Opt. Soc., Rapid publ. **17** (2021), no. 23, 1–28.
26. A. G. Ramm, *A simple proof of the Fredholm alternative and a characterization of the Fredholm operators*, The American Mathematical Monthly **108** (2001), no. 9, 855–860.
27. P. S. Westbrook, K. S. Feder, T. Kremp, T. F. Taunay, E. Monberg, J. Kelliher, R. Ortiz, K. Bradley, K. S. Abedin, D. Au, and G. Puc, *Integrated optical fiber shape sensor modules based on twisted multicore fiber grating arrays*, Optical Fibers and Sensors for Medical Diagnostics and Treatment Applications XIV (Israel Gannot, ed.), vol. 8938, International Society for Optics and Photonics, SPIE, 2014, pp. 88–94.
28. Paul Westbrook, K.S. Feder, Tristan Kremp, W. Ko, Hongchao Wu, E. Monberg, Debra Simoff, and K. Bradley, *Distributed sensing over meter lengths using twisted multicore optical fiber with continuous Bragg gratings*, Furukawa Review (2017), 26–32.

Department of Mathematics, Southern Methodist University, Dallas, TX 75275, USA
Email address: rhparker@smu.edu

Department of Mathematics, University of Kansas, Lawrence, KS 66045, USA
Email address: yshen@ku.edu

Department of Mathematics, Southern Methodist University, Dallas, TX 75275, USA
Email address: aaceves@smu.edu

Department of Mathematics, The University of Texas at Dallas, Richardson, TX 75080, USA
Email address: zweck@utdallas.edu